The nano-epsilon dot method for strain rate viscoelastic characterisation of soft biomaterials by spherical nano-indentation

G. Mattei [a], G. Gruca [b], N. Rijnveld [b] and A. Ahluwalia [a,*]

[a] Research Centre "E. Piaggio", University of Pisa, Largo Lucio Lazzarino 1, 56122 Pisa, Italy

[b] Optics11, De Boelelaan 108, 1081 HV Amsterdam, The Netherlands

[*]Corresponding Author

Address: Research Centre "E. Piaggio", University of Pisa, Largo Lucio Lazzarino 1, 56122 Pisa, Italy

Tel: +39 050 2217056

Fax: +39 050 2217051

E-mail: arti.ahluwalia@centropiaggio.unipi.it

Abstract

Nano-indentation is widely used for probing the micromechanical properties of materials. Based on the indentation of surfaces using probes with a well-defined geometry, the elastic and viscoelastic constants of materials can be determined by relating indenter geometry and measured load and displacement to parameters which represent stress and deformation.

Here we describe a method to derive the viscoelastic properties of soft hydrated materials at the micro-scale using constant strain rates and stress-free initial conditions. Using a new self-consistent definition of indentation stress and strain and corresponding unique depth-independent expression for indentation strain rate, the epsilon dot method, which is suitable for bulk compression testing, is transformed to nano-indentation. We demonstrate how two materials can be tested with a displacement controlled commercial nano-indentor using the nano-espilon dot method (nano-$\dot{\varepsilon}M$) to give values of instantaneous and equilibrium elastic moduli and time constants with high precision. As samples are tested in stress-free initial conditions, the nano-$\dot{\varepsilon}M$ could be useful for characterising the micro-mechanical behaviour of soft materials such as hydrogels and biological tissues at cell length scales.

Keywords: nano-indentation, epsilon dot method, strain rate, mechanical properties, viscoelastic models, soft materials

1. Introduction

Nano-indentation is emerging as a popular technique for the mechanical characterisation of biological and biomimetic materials (Ebenstein and Pruitt, 2006; Oyen, 2013). Typically, a probe is brought in contact with a surface, pushed into the material and then retracted, recording load (P) and displacement (h) over time (t). The P-h-t data are then analysed with a range of models, such as elastic, elastoplastic, viscoelastic or poroviscoelastic, to derive material mechanical properties (Oyen and Cook, 2009). Most commercial nano-indentation systems come with an automated x-y stage that allows several measurements over the surface of the sample and spatial mapping of its local mechanical properties (Constantinides et al., 2006). There are several reasons that motivate the use of indentation at small, typically cell length, scales for characterising the mechanical properties of natural materials. First of all, this method is ideal for probing local gradients and heterogeneities typical of natural materials and investigating their hierarchical multi-scale organization (Cuy et al., 2002). Moreover, it does not require extensive sample preparation prior to testing (in contrast with most classical techniques, e.g. tensile testing which requires "dog-bone" shaped samples) and allows the measurement of very small forces and displacements (generally in the range of μN ÷ mN and nm ÷ μm, respectively) (Gentleman et al., 2009). Nano-indentation requires small volumes of materials, and is thus particularly suitable for valuable samples (Olesiak et al., 2010). Furthermore, a variety of deformation modes can be studied by changing experimental time scales, indenter tip geometry and loading conditions. Because very small forces are applied, the technique is well suited for soft biomaterials (Karimzadeh and Ayatollahi, 2014; Rettler et al., 2013), such as hydrogels (Ebenstein and Pruitt, 2004; Kaufman et al., 2008), which due to their pliable and highly hydrated nature, are a challenge to characterise using macro-scale techniques. Finally, given that pathological and ageing tissues are known to exhibit altered mechanical properties (Derby and Akhtar, 2015; DeWall et al., 2012), this method is also attractive in the biomedical context as a potential diagnostic tool or for intelligent scaffold design (Albert et al., 2013; Lyyra et al., 1995; Mattei et al., 2015).

The commercialization of indentation instruments has led to the optimisation of testing and analyses methods for deriving material elastic and plastic properties, such as elastic modulus and hardness. However, the constitutive response of soft tissues and biomaterials differs from that of linearly elastic and isotropic engineering materials. First, the former generally exhibit non-linear stress-strain (σ-ε) behaviour (Hollister et al., 2011; Mattei et al., 2014); second, their mechanical response is often characterised by a significant time-dependence, which is typically described by empirical lumped parameter viscoelastic models (Galli et al., 2011a, 2011b; Raghunathan et al., 2010); third, these materials are likely to be both macroscopically and microscopically anisotropic, especially in case of biological tissues (Chen et al., 2015). Therefore, blindly testing these materials with commercial nano-indenters that return elastic and plastic properties is generally reductive and unlikely to provide an accurate description of their mechanical behaviour.

The vast majority of nano-indentation tests are based on a single loading-unloading cycle and may include a holding phase at peak load or indentation depth, which can be useful to characterise the creep or relaxation behaviour of time-dependent materials. Indentation is usually performed at a constant loading or displacement rate, or using an exponentially increasing load over time to obtain a constant indentation strain rate (Lucas et al., 2011; Oyen and Cook, 2003). Among the approaches proposed to date, the Oliver-Pharr method introduced in the early 1990s (Oliver and Pharr, 1992) has been widely used to analyse indentation data and derive material properties. This method is based on an elastic-plastic contact model and uses three key parameters from the indentation test, namely the peak indenter force (P_{max}), the peak indenter displacement (h_{max}) and the unloading slope or stiffness ($S = \partial P/\partial h$). The analysis is carried out on either the entire unloading curve or the infinitesimal unloading portion of sinusoidal oscillations performed at the top of the loading curve. Materials with time-independent mechanical properties can be successfully tested with this method. However, it is not suited for time-dependent materials, since their continuing deformation invalidates the assumption of elastic unloading (Lin and Hu, 2006). Indeed, when unloading a creeping material in load-control mode, the resultant unloading slope can be near vertical or even

negative as the forward-going displacement due to creep overwhelms the elastic recovery (Oyen and Cook, 2003). A number of experimental and numerical ploys (including trying to exhaust the creep prior to unloading with a long holding time at peak force (Galli et al., 2011a; Hu et al., 2010) or trying to outpace the creep by unloading quickly (Chiravarambath et al., 2009)) have been proposed to solve this issue and correct the unloading slope to use Oliver-Pharr analyses on creeping materials. However, all these methods are aimed at removing the effect of creep and characterise the material elastic properties only.

An alternative testing mode is dynamic nano-indentation, the micro-scale equivalent of dynamic mechanical analysis (DMA) typically performed at the macro-scale. This technique relies on the establishment of a small but measurable initial contact force to trigger the indenter oscillation and data acquisition, which may cause significant pre-stress and be detrimental to soft hydrated materials and biological tissues (Mattei et al., 2014). One example of dynamic nano-indentation is the "continuous stiffness measurement" technique (CSM), in which stiffness is measured continuously while indenting by imposing a small dynamic oscillation on the force (or displacement) signal and measuring the amplitude and phase of the corresponding displacement (or force) signal (Li and Bhushan, 2002). This technique has been widely used in the literature (Bouaita et al., 2006; Franke et al., 2011; Hayes et al., 2011): it reduces the reliance on unloading curves and offers several advantages, such as providing results as a function of indentation depth, reducing the time required for calibration and testing procedures, and avoiding the effects of time-dependent plasticity and thermal drift at high frequencies (Li and Bhushan, 2002; Oliver and Pharr, 2004).

The use of the loading portion of the load-displacement curve, instead of the classical unloading portion used in the Oliver-Pharr approach, is far more suitable for soft, hydrated materials. In particular, the mechanical properties derived from the loading portion of the curve are representative of those of the virgin material, returning a constant modulus value regardless of the maximum load (or displacement) chosen for the measurements. Conversely, the modulus value

obtained from the unloading curve is likely to increase with increasing maximum indentation load (or displacement), as expected when going beyond the sample linear elastic (or viscoelastic) region (Pathak et al., 2008a). Moreover, during unloading it is assumed that only the elastic displacements are recovered (Oliver and Pharr, 2004), thus methods based on the unloading curve are unsuitable for testing viscoelastic materials.

Commercial nano-indenters generally operate in load control mode (i.e. controlling the force applied to the sample) and use a load-based contact determination method by measuring either a small force on the sample or a small change in the apparent stiffness (i.e. an instantaneous reading of $S = \partial P/\partial h$) (Kaufman and Klapperich, 2009). Although these techniques work well in case of stiff elastic materials, they are problematic when testing compliant and time-dependent materials, where even a small "trigger" load of few μN can cause a significant indenter displacement into the sample (which, also increases with time after contact). In an ideal indentation test, particularly for soft biological tissues and hydrogels, the P-h-t acquisition should start prior to contact with the sample (Kaufman et al., 2008; Mattei et al., 2014; Tirella et al., 2014). This can be easily done with displacement-controlled experiments by locating the surface with the probe, lifting it off and starting the indentation cycle just above the sample, after leaving the material enough time to recover at the site of initial contact. Most reports define the point of contact as the position on the loading curve at which the tip snaps into contact (Cao et al., 2011). However, the snap into contact may be not clearly visible on load-displacement curve when testing soft biological tissues or hydrogels, requiring other definitions to identify the contact point. Kaufman et al. proposed determining the contact point as the point of lowest force on the unloading curve (Kaufman et al., 2008). In this study we define the contact point as the last point at which the load crosses the abscissa of the load-displacement curve during loading (Mattei et al., 2014; Tirella et al., 2014). This definition allows us to uniquely identify the point of contact when the snap into contact is not clearly evident or in the presence of noise around zero load.

We recently proposed a method, called the "epsilon dot method" ($\dot{\varepsilon}M$), to characterise material viscoelastic properties through short compressive tests at different strain rates, without the need of any load-trigger and/or long testing trials. (Tirella et al., 2014). Briefly, it is based on performing a series of short compressive tests at different strain rates while acquiring force and displacement data versus time within the material linear viscoelastic region (LVR). The acquisition of force and displacement time-series starts with the probe of the testing device close to but not in contact with the sample surface to guarantee a zero pre-stress initial condition and a constant testing velocity. Experimental force and displacement time-series are normalised to the sample cross-sectional area and initial thickness measured just prior to testing, thus obtaining stress and strain time-series. Then, stress-time data within the LVR (defined as the region in in which stress varies linearly with applied strain to within $R^2 > 0.99$) obtained from measurements at different strain rates are used to derive viscoelastic constants for lumped parameter models using a global fitting procedure.

In this paper we describe a variant of the $\dot{\varepsilon}M$ suitable for nano-indentation measurements (the nano-epsilon dot method or nano-$\dot{\varepsilon}M$), which resolves some of the issues (use of the unloading portion and load triggering and control) related to the nano-scale testing of soft viscoelastic materials. The nano-$\dot{\varepsilon}M$ is applied to two different materials: polydimethylsiloxane (PDMS) and gelatin hydrogels. PDMS is a widely used elastomer with well documented viscoelastic properties (Gray et al., 2003; Lin et al., 2009). Gelatin hydrogels are characterised by a highly hydrated three-dimensional network similar to soft tissues and are commonly used in many biomedical applications. Their viscoelastic and strain rate dependent properties are amply reported in the literature (Bigi et al., 2001; Kalyanam et al., 2009; Kwon and Subhash, 2010; Martucci et al., 2006). The viscoelastic parameters estimated using the nano-$\dot{\varepsilon}M$ are also related to those we previously obtained testing these materials in unconfined compression with the original $\dot{\varepsilon}M$ (Tirella et al., 2014) in order to compare bulk and surface mechanical properties.

2. Material and methods

2.1. Conversion of indentation load-displacement to stress-strain

Despite the fact that conversion of load-displacement curves to indentation stress-strain is almost as old as the technique of using indentation to probe the mechanical properties of solids (Tabor, 1951), there is still no consensus about the definition of stress and strain, likely due to the widespread use of the Oliver-Pharr method based on P-h-t data. During the 1990s, Field and Swain proposed a method to obtain indentation stress-strain curves from load-displacement curves (Field and Swain, 1995, 1993), however their methodology was not caught on, with a few exceptions (Basu et al., 2006; Haghshenas and Klassen, 2013; Herbert et al., 2001; Pathak et al., 2008a). The majority of studies dealing with indentation strain rate define it as $\dot{\varepsilon}_{ind} = \dot{h}/h$ (i.e. the instantaneous displacement rate of the indenter divided by the instantaneous displacement into the surface) and use a loading scheme with exponentially increasing load over time to obtain constant $\dot{P}/P$, resulting in constant $\dot{\varepsilon}_{ind}$ (Haghshenas and Klassen, 2013; Maier et al., 2011; Shen et al., 2012). However, this definition does not represent the time derivative of the indentation strain (ε_{ind}). The latter is generally defined as $\varepsilon_{ind} = a/R$, where $a = \sqrt{Rh}$ is the depth-dependent radius of contact and R represents the radius of the spherical indenter tip as illustrated in Fig 1 (Basu et al., 2006; Field and Swain, 1993). Hence the resulting strain rate should be $\dot{\varepsilon}_{ind} = \dot{h}/2\sqrt{Rh}$, giving a depth-dependent function that is very different from the depth-independent classical engineering strain rate defined as $\dot{\varepsilon} = \frac{\partial}{\partial t}\left(\frac{l(t)-l_0}{l_0}\right) = \frac{v(t)}{l_0}$ (l_0 and $l(t)$ are respectively the original sample length and the length at time t, while $v(t)$ represents the testing speed, or displacement rate).

Based on these considerations, to translate the $\dot{\varepsilon}M$ approach from bulk material testing to nano-indentation measurements we propose here a new definition of indentation stress (σ_{ind}) and strain (ε_{ind}) that allows us to obtain indentation stress-strain curves at constant strain rates (defined as $\dot{\varepsilon}_{ind} = \partial\varepsilon_{ind}/\partial t$) from load-displacement measurements at constant displacement rate ($\dot{h}$). It is worth noting that Pathak et al. (Pathak et al., 2008b) have quite recently proposed a new definition

of indentation strain as $\varepsilon_{ind} = \frac{4}{3\pi}\frac{h}{a}$, but it is not suitable for our purposes since its time derivative is proportional to $\dot{h}/h$ and is thus not constant during the test but dependent on the indentation depth.

The analysis of spherical nano-indentation data is generally based on the Hertz model (Fig. 1 and Eq. 1), assuming a linear elastic and isotropic material response (Field and Swain, 1995, 1993; Oliver and Pharr, 2004; Pathak et al., 2008b). The load *P* is expressed as:

$$P = \frac{4}{3} E_{eff} R^{1/2} h^{3/2} \tag{1}$$

where R is the radius of the spherical indenter tip, h is the penetration depth and E_{eff} denotes the effective composite elastic modulus of the indenter and specimen system given by

$$\frac{1}{E_{eff}} = \frac{1-\upsilon^2}{E} + \frac{1-\upsilon'^2}{E'} \tag{2}$$

In Eq. 2, E' and υ' respectively refer to the modulus and Poisson's ratio of the indenter, while the other terms refer to those of the sample. In case of soft materials, where $E' \gg E$, Eq. 2 can be approximated as follows:

$$\frac{1}{E_{eff}} \approx \frac{1-\upsilon^2}{E} \tag{3}$$

For a rigid spherical indenter, Sneddon (Sneddon, 1965) showed that the elastic displacements of a plane surface above and below the circle of contact are equal and given by $h/2$, with

$$h = \frac{a^2}{R} \tag{4}$$

where a denotes the contact radius during indentation (Fig. 1). Combining Eqs. 1 and 4 yields

$$\frac{P}{\pi a^2} = \frac{4}{3\pi} E_{eff} \left(\frac{a}{R}\right) \tag{5}$$

The left side of Eq. 5 is referred to as the indentation stress (σ_{ind}) or mean contact pressure, while a/R on the right side represents the indentation strain (ε_{ind}) (Field and Swain, 1993).

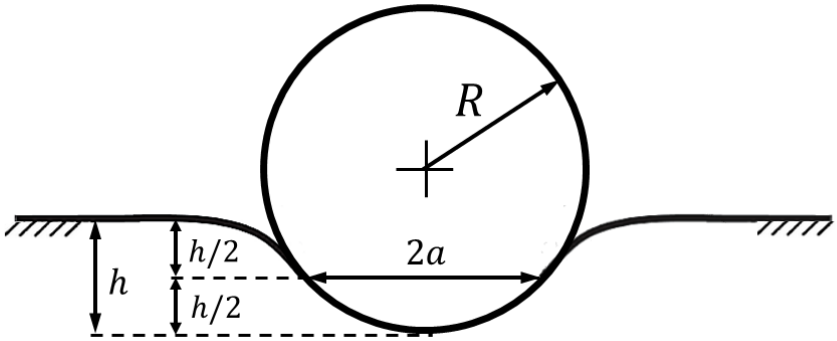

Fig. 1*: Schematic representation of elastic (Hertzian) spherical indentation.*

Since the nano-$\dot{\varepsilon}M$ requires indentation stress-time series recorded at constant indentation strain rates, Eq. 5 can be rearranged multiplying both sides by $h/\sqrt{hR} = h/a$, thus obtaining an indentation strain which is linearly related to the displacement into surface (h).

$$\frac{P}{R\sqrt{hR}} = \frac{4}{3}E_{eff}\left(\frac{h}{R}\right) \approx \frac{4}{3}\left(\frac{E}{1-\upsilon^2}\right)\left(\frac{h}{R}\right) \tag{6}$$

According to Eq. 6 we define the indentation stress and strain as follows (Eqs. 7 and 8, respectively).

$$\sigma_{ind} = \frac{P}{R\sqrt{hR}} \tag{7}$$

$$\varepsilon_{ind} = \frac{4}{3(1-\upsilon^2)}\left(\frac{h}{R}\right) \tag{8}$$

This definition has several advantages, in particular:

1. The ratio $\sigma_{ind}/\varepsilon_{ind}$ directly returns the sample modulus E (in case of fairly soft materials, where $E' \gg E$), without the need of any multiplicative factor;

2. The constant indentation strain rate ($\dot{\varepsilon}_{ind}$) does not depend on the indentation h but only on the indenter velocity ($\dot{h}$). In fact, by using a constant indenter velocity, the displacement into surface is simply given by $h = \dot{h} \cdot t$ and consequently

$$\dot{\varepsilon}_{ind} = \frac{\partial \varepsilon_{ind}}{\partial t} = \frac{4}{3(1-\upsilon^2)}\left(\frac{\dot{h}}{R}\right) = \text{constant during test} \quad (9)$$

Therefore, indentation stress and strain time-series for the nano-$\dot{\varepsilon}M$ can be easily obtained from indentation measurements by setting an appropriate indenter velocity ($\dot{h}$) to obtain the desired $\dot{\varepsilon}_{ind}$, and calculating σ_{ind} and ε_{ind} from measured load (P) and displacement (h) data according to Eqs. 7 and 8, respectively. Subsequently, the stress-time series obtained can be analysed with the $\dot{\varepsilon}M$ approach to obtain material viscoelastic constants using the global fitting procedure reported in Tirella et al. (Tirella et al., 2014). In this paper we describe the application of the nano-$\dot{\varepsilon}M$ to viscoelastic characterisation of PDMS and gelatin hydrogels.

2.2. Experimental details

PDMS samples with flat surfaces were obtained by casting a Sylgard 184 pre-polymer solution (Dow Corning, Wiesbaden, Germany; 10:1 base to catalyst ratio, prepared as per manufacturer's instructions and degassed for 30 min to remove air bubbles) into 3 mm height – 5 mm diameter cylindrical moulds. After 1 h curing at 60 °C, samples were removed from the moulds and ready for testing.

Gelatin samples were prepared using a 5 % w/v gelatin solution obtained dissolving type A gelatin powder (G2500, Sigma-Aldrich, Milan, Italy) in deionised water at 50 °C under stirring for 2 h. Samples with flat surfaces were obtained by casting the gelatin solution into the same cylindrical

moulds used for PDMS and allowing them to physically crosslink at room temperature for 1 h. Gelled samples were then removed from the moulds and stored at 4 °C.

Nano-indentation tests were carried out using the displacement-controlled PIUMA Nanoindenter (Optics11, Amsterdam, The Netherlands) (Chavan et al., 2012). Two different spherical tips with radii of 64 (cantilever stiffness, k = 13.4 N/m) and 70 μm (k = 0.550 N/m) were used to test PDMS and gelatin samples, respectively. All measurements were performed by gluing samples onto the bottom of a Petri dish and then submerging them in deionised water at room temperature with the nano-indenter tip remaining well below the surface of water at all times in order to avoid any error introduced by strong adhesive forces at the air-water interface (Kaufman et al., 2008).

To ensure a repeatable testing state, gelatin samples were left submerged for enough time in order to swell to equilibrium and attain room temperature prior to testing. The Petri dish containing the sample was mounted on top of the PIUMA sample stage which is moved by piezo-stepper motors. In order to avoid sample pre-stress and subsequent errors in estimating the mechanical properties, the P-h-t acquisitions were started with the cantilever tip just above the sample. In particular, the probe was brought close to the sample surface by using a coarse-fine stepping and scanning algorithm. Specifically, vertical steps by the coarse positioner were followed by 1 μm "pokes" of the indentation piezostack, until the location of the sample surface was determined within 1 μm accuracy. At this point, the indenter probe was lifted off the surface by retracting it a few microns and then translating it laterally by 200 μm, such that the indentation cycle started from a non-contact position.

Based on the ferrule-top optomechanical fiber sensor, the PIUMA Nanoindenter calculates the indentation depth into the sample as

$$h = d_p - d_c \tag{10}$$

where d_p denotes the displacement of the z-piezoelectric translator, which drives the cantilever and sample displacement, and d_c represents the cantilever deflection measured by the interferometer (Chavan et al., 2012). Notably, both the indentation depth into the sample (h) and the cantilever deflection depend on several parameters such as the cantilever stiffness (k), the spherical tip radius (R) and, obviously, the sample stiffness. For example, h is null while indenting very stiff (i.e. with stiffness >> k) samples that do not deform while being indented, such as glass (Chavan et al., 2012).

Using the PIUMA, only the z-piezo displacement rate ($\dot{d_p}$) can be user-defined to obtain a given total indentation strain rate of the cantilever-sample system ($\dot{\varepsilon}_t$) while the actual $\dot{\varepsilon}_{ind}$ experienced by the sample (which is dependent on several factors such as k, R and sample stiffness) has to be derived post measurement. As outlined in Supplementary Information SI 1, given the elastic nature of the cantilever, a constant $\dot{d_p}$ results in a constant $\dot{h}$ and hence a constant $\dot{\varepsilon}_{ind}$ while testing viscoelastic samples within the LVR. As a consequence, setting a constant piezo displacement velocity will result in a constant total strain rate of the cantilever-sample system ($\dot{\varepsilon}_t$). Thus the value of $\dot{d_p}$ which yields the desired $\dot{\varepsilon}_t$ was calculated using Eq. 9, substituting $\dot{\varepsilon}_{ind}$ and $\dot{h}$ with $\dot{\varepsilon}_t$ and $\dot{d_p}$ respectively, considering the samples as incompressible materials with υ = 0.5 (Khanafer et al., 2009; Radmacher et al., 1995). The constant indentation strain rate experienced by the sample ($\dot{\varepsilon}_{ind}$) can be obtained from the slope of ε_{ind} over time obtained from indentation measurements and used in the $\dot{\varepsilon}M$ analysis to derive un-biased material viscoelastic properties.

Specifically, PDMS was tested at $\dot{\varepsilon}_t$ = 0.056, 0.074, 0.111, 0.222 s^{-1}, while gelatin was tested at $\dot{\varepsilon}_t$ = 0.025, 0.05, 0.1, 0.25 s^{-1}. Each indentation test consisted of a single displacement-controlled loading-unloading cycle up to 20 µm depth. Tests at different indentation strain rates were performed on different points of the sample surface (spaced 200 µm) in order to avoid any error due to repeated testing cycles. For each strain rate, n = 10 independent measurements were carried out.

2.3. Lumped parameter estimation

Both samples were treated as mechanically isotropic materials (Tirella et al., 2014). The initial contact point was identified as the last point at which the load crosses the abscissa of the loading portion of the load-displacement indentation curve towards monotonically increasing values (Mattei et al., 2014; Tirella et al., 2014). Experimental P-h-t data were offset to be zero in correspondence with this point. Load and displacement data were converted into indentation stress (σ_{ind}) and strain (ε_{ind}) according to Eqs. 7 and 8, and sample LVR identified as the region in which stress varies linearly with applied strain ($R^2 > 0.99$). Then, stress-time data within LVR obtained from measurements at different indentation strain rates were analysed using the $\dot{\varepsilon}M$ global fitting procedure with shared parameters to derive material viscoelastic constants for lumped parameter models combining pure springs and dashpots in different configurations. For the sake of comparison with previous results published in Tirella et al. (Tirella et al., 2014), the same two models, i.e. the Maxwell Standard Linear Solid (SLS) and the 2-arm Generalised Maxwell model (GM2), were used to estimate the material viscoelastic coefficients with the $\dot{\varepsilon}M$ global fitting approach (S1 2 and SI 3). In order to select suitable initial guesses for the viscoelastic parameters to estimate, an annealing scheme based on multiplying and dividing each initial parameter by 10 while keeping the instantaneous modulus at a constant value (i.e. a constant sum of all springs in the model) was adopted. This approach allows reliable and absolute material viscoelastic parameters to be obtained, avoiding most of the local minima during the fitting procedure. The minimum parameter value was constrained to zero to prevent the fitting procedure returning negative values for the estimated viscoelastic coefficients. Comparisons between parameter values were made using the Student's t-test, setting significance at $p < 0.05$.

3. Results

The LVR was determined as described in Section 2.3 and extended up to a strain of 0.10 for both materials. Experimental stress-strain series obtained testing both PDMS and gelatin samples at various total indentation strain rates ($\dot{\varepsilon}_t$) are shown in Fig. 2, reporting only data within the LVR. As expected, gelatin exhibits a more pronounced rate-dependent behaviour than PDMS, with increase in apparent elastic modulus with applied strain rate (Table 1).

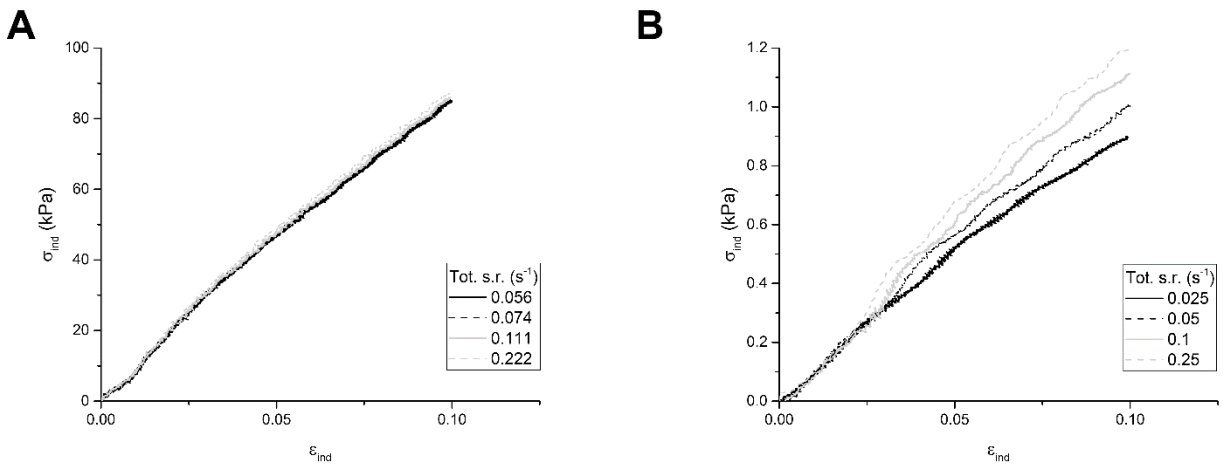

Fig. 2: *Indentation stress-strain curves obtained testing PDMS (A) and gelatin (B) samples at different total indentation strain rates ($\dot{\varepsilon}_t$). The rate-dependent behaviour is reflected in the increase of apparent elastic modulus, which is more evident for gelatin samples than PDMS.*

Tab. 1: *Actual indentation strain rates ($\dot{\varepsilon}_{ind}$) and apparent elastic moduli (E_{app}) obtained for PDMS and gelatin samples tested at different total indentation strain rates ($\dot{\varepsilon}_t$). Values are reported as mean ± standard deviation.*

Sample	**$\dot{\varepsilon}_t$ (s^{-1})**	**$\dot{\varepsilon}_{ind}$ (s^{-1})**	**E_{app} (kPa)**
PDMS	0.056	$0.019 \pm 2.50 \cdot 10^{-4}$	881.6 ± 14.7
	0.074	$0.026 \pm 1.96 \cdot 10^{-4}$	887.7 ± 10.2
	0.111	$0.039 \pm 2.08 \cdot 10^{-4}$	894.9 ± 10.0
	0.222	$0.077 \pm 2.10 \cdot 10^{-4}$	921.9 ± 5.91
Gelatin	0.025	$0.015 \pm 2.53 \cdot 10^{-4}$	9.34 ± 0.27
	0.05	$0.028 \pm 4.12 \cdot 10^{-4}$	10.71 ± 0.28
	0.1	$0.056 \pm 4.03 \cdot 10^{-4}$	11.76 ± 0.24
	0.25	$0.14 \pm 2.92 \cdot 10^{-3}$	12.53 ± 0.21

Indentation strain versus time plots within LVR obtained at different total strain rates for both PDMS and gelatin samples are reported in Fig. 3, showing that constant total indentation strain rates ($\dot{\varepsilon}_t$) result in constant actual indentation strain rates experienced by the sample ($\dot{\varepsilon}_{ind}$), as expected (Supplementary Information SI 1).

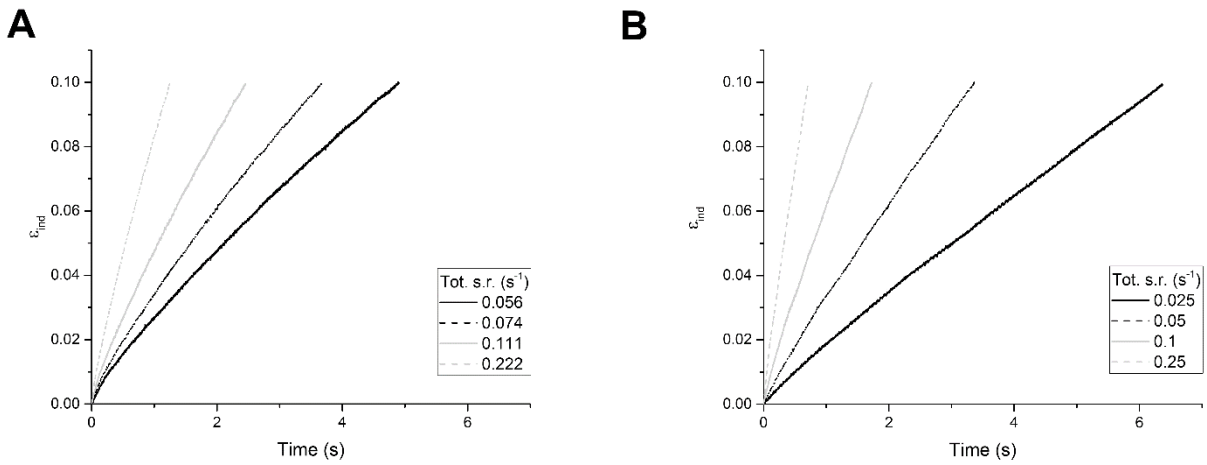

Fig. 3: *Indentation strain-time curves obtained testing PDMS (A) and gelatin (B) samples at different total indentation strain rates ($\dot{\varepsilon}_t$). The slope of these curves returns the actual indentation strain rate experienced by the sample tested with a cantilever-based device ($\dot{\varepsilon}_{ind}$).*

The $\dot{\varepsilon}_{ind}$ values, derived as the slope of the ε_{ind} versus time, are reported in Table 1, along with the respective apparent elastic moduli obtained for both materials investigated in this work. Notably, the $\dot{\varepsilon}_{ind}$ values obtained were very precise, with coefficient of variations (i.e. ratios between standard deviations and respective mean values) less than 2 %. As explained in SI 1, $\dot{\varepsilon}_{ind}$ obtained in this way is less than the total strain rate $\dot{\varepsilon}_t$.

Stress-time series in the LVR are shown in Fig. 4 for both samples investigated. Since the LVR was within 0.10 strain for all experiments, the higher the strain rate the shorter the duration of the stress-time series.

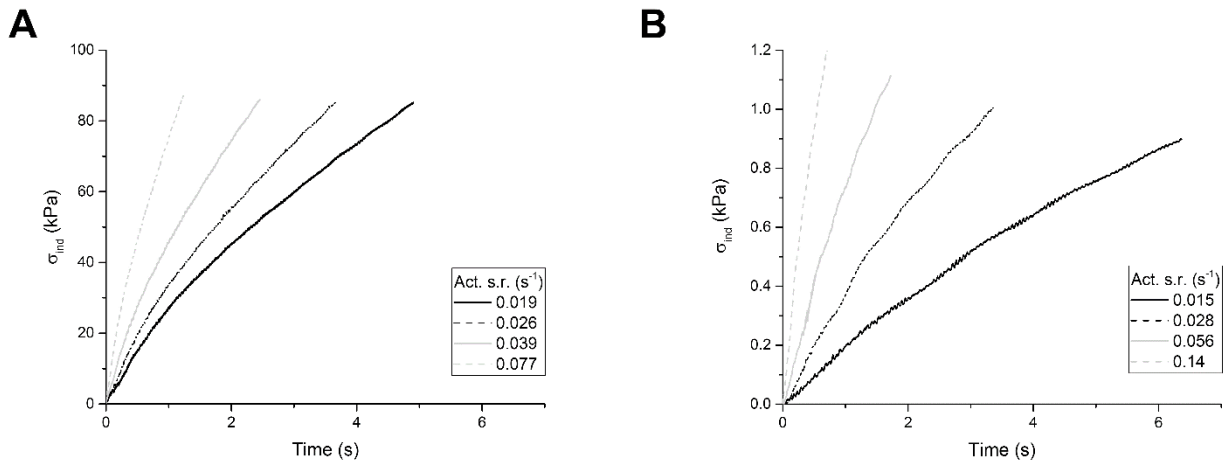

Fig. 4: *LVR stress-time curves at different indentation strain rates ($\dot{\varepsilon}_{ind}$) obtained for PDMS (A) and gelatin (B) samples.*

The fitting results for Maxwell SLS and GM2 models are summarised in Table 2, where E_{inst} and E_{eq} represent the instantaneous (i.e. sum of all springs in the model) and equilibrium (E_0) moduli, respectively, while τ_i is the i^{th}-arm characteristic relaxation time, calculated as η_i/E_i. Although convergence was obtained for both SLS and GM2 models, fitting the datasets to the latter yielded non-significant results with meaningless values and/or very large standard errors of estimation, clearly indicating model over-parameterisation.

Tab. 2: *Viscoelastic parameters of PDMS and gelatin samples estimated for Maxwell SLS and GM2 lumped models using the nano-$\dot{\varepsilon}M$. Results are expressed as estimated parameter value ± standard error. The GM2 parameters τ_2 and E_{eq} reported in italics cannot be considered as significant as their values are almost meaningless with very large standard errors.*

	PDMS		**Gelatin**	
Parameter	*Maxwell SLS*	*GM2*	*Maxwell SLS*	*GM2*
E_{inst} (kPa)	$1.74 \cdot 10^3 \pm 1.47 \cdot 10^1$	$1.74 \cdot 10^3 \pm 1.02 \cdot 10^2$	14.08 ± 0.58	$\mathit{14.08 \pm 1.37 \cdot 10^3}$
E_{eq} (kPa)	$8.82 \cdot 10^2 \pm 8.72 \cdot 10^{-1}$	$5.98 \cdot 10^2 \pm 7.14 \cdot 10^1$	1.84 ± 0.42	$\mathit{4.07 \cdot 10^{-4} \pm 4.65 \cdot 10^2}$
τ_1 (s)	$0.26 \pm 4.93 \cdot 10^{-3}$	$0.26 \pm 4.93 \cdot 10^{-3}$	6.90 ± 0.60	$\mathit{14.78 \pm 2.36 \cdot 10^3}$
τ_2 (s)	-	$\mathit{1.04 \cdot 10^{12} \pm 3.68 \cdot 10^{11}}$	-	$\mathit{5.57 \pm 1.36 \cdot 10^3}$
R^2	0.97	0.97	0.99	0.99

4. Discussion

The challenges of current nano-indentation testing and data analysis for accurate determination of the viscoelastic properties of soft tissues and biomaterials have been amply addressed in the introduction. The nano-$\dot{\varepsilon}M$, stemming from the $\dot{\varepsilon}M$ (Tirella et al., 2014), was developed to overcome some of these challenges. Based on a new definition of indentation stress and strain, the method uses constant indentation strain rates to derive viscoelastic parameters of materials starting from zero initial stress.

In this work, we used the PIUMA Nanoindenter, one of the few commercially available displacement-controlled nano-indentation instruments. Despite the fact that the desired sample indentation strain rate can only be set indirectly, it is ideally suited for the application of constant indentation strain rates as defined in the nano-$\dot{\varepsilon}M$. Furthermore its ferrule-top cantilever offers several advantages when testing samples submerged in a liquid medium, since the force due to the

water meniscus on the shaft of classical indenters makes the analysis of indentation data more complicated (Chavan et al., 2012; Mann and Pethica, 1996).

The nano-$\dot{\varepsilon}M$ was used to analyse the viscoelastic properties of gelatin and PDMS. The results obtained show that the viscoelastic behaviour of both materials within LVR can be represented by a Maxwell SLS model. Using a five-parameter GM2 model results in an over-parameterisation of viscoelastic behaviour for both materials, as demonstrated by the almost meaningless values of τ_2 and E_{eq} respectively obtained for PDMS and gelatin, as well as by the several large standard errors of estimation reported in Table 2. In fact, the estimated instantaneous modulus (E_{inst}) does not change between SLS and GM2 models for either material, as previously observed in Mattei et al. (Mattei et al., 2014), while the other parameters change significantly, except for the gelatin τ_1.

As reported in Table 3, we obtained good agreement between the elastic moduli estimated at the micro- (nano-$\dot{\varepsilon}M$) and the macro-scale ($\dot{\varepsilon}M$) for gelatin (Tirella et al., 2014). In particular, the instantaneous (E_{inst}) and equilibrium moduli (E_{eq}) change by +25% and -25% between micro- and macro-scale testing, respectively. These results are consistent with those reported by Kaufmann et al. (Kaufman et al., 2008) who tested poly(2-hydroxyethyl methacrylate) hydrogels both through nano-indentation and unconfined compression experiments. Simha et al. (Simha et al., 2007) also showed that the elastic moduli of urethane obtained with nano-indentation and unconfined compression tests are similar.

Tab. 3: *Comparison between Maxwell SLS viscoelastic parameters of PDMS and gelatin samples obtained at the micro- and the macro-scale using the nano-$\dot{\varepsilon}M$ and the $\dot{\varepsilon}M$, respectively. Results at the macro-scale were taken from Tirella et al.* (Tirella et al., 2014).

	PDMS		**Gelatin**	
Parameter	*Micro-scale (nano-$\dot{\varepsilon}M$)*	*Macro-scale ($\dot{\varepsilon}M$)*	*Micro-scale (nano-$\dot{\varepsilon}M$)*	*Macro-scale ($\dot{\varepsilon}M$)*
E_{inst} (kPa)	$(1.74 \pm 0.01)\cdot 10^3$	$(2.55 \pm 0.04)\cdot 10^3$	14.08 ± 0.58	11.23 ± 0.45
E_{eq} (kPa)	$(8.82 \pm 0.01)\cdot 10^2$	$(2.14 \pm 0.01)\cdot 10^3$	1.84 ± 0.42	2.43 ± 0.10
τ_1 (s)	0.26 ± 0.01	0.66 ± 0.25	6.90 ± 0.60	4.85 ± 0.19

In case of PDMS, both the E_{inst} and the E_{eq} at the micro-scale were found to be lower than those obtained at the macro-scale, changing by -32% and -59%, respectively.

The Maxwell SLS characteristic relaxation time (τ_1) of gelatin at the micro-scale was found to be higher than that obtained at the macro-scale (+ 42%), while that of PDMS was found to be lower (-61%). Kaufman et al. (Kaufman et al., 2008), report significantly lower time constants in nano-indentation with respect to unconfined compression, as well as with Sasaki et al. (Sasaki, 2004) and Mak et al. (Mak et al., 1987), suggesting that relaxation rate is dependent on test geometry. In particular, Sasaki et al. reported that the relaxation time constant for poly (N-isopropryl acrylamide) hydrogel is proportional to the square of sample radius, while Mak et al. showed that nano-indentation experiments with larger indenter tips took longer to reach equilibrium than those with smaller indenter tips. As a consequence, since the sampled region in nano-indentation experiments is generally much smaller than the entire sample surface area, we would expect the resultant time constants to be smaller than those obtained in unconfined compression.

It is important to note that some of the variations in viscoelastic constants between nano-indentation and unconfined compression may be due to real differences between the bulk and the surface

mechanical properties (Kaufman et al., 2008), or due to the fact that material constituents may creep at different scales (Eberhardsteiner et al., 2014; Scheiner and Hellmich, 2009). In addition, it is worth underlining that nano-indentation stress and strain definitions considered here as well as in other nano-indentation reports (e.g. (Basu et al., 2006; Haghshenas and Klassen, 2013; Herbert et al., 2001; Pathak et al., 2008a)) are not the same as the bulk engineering stress ($\sigma = F/A$) and strain ($\varepsilon = \Delta l/l_0$) used to analyse tensile and compressive data from uniaxial tests, with obvious implications on the derived results. In view of these considerations, caution should be exercised when interpreting differences or similarities between results obtained at different length scales. Rather scientists should focus on obtaining consistent and reproducible material characteristics by designing standardised measurement and sample preparation protocols accompanied by robust and meaningful data analysis methods.

5. Conclusions

The nano-$\dot{\varepsilon}M$ described in this paper combines the advantages of the $\dot{\varepsilon}M$ approach (e.g. absence of sample pre-stress and degradation) with those of conventional nano-indentation techniques (e.g. derivation of local material properties point to point at characteristic cellular length scales). These features render it highly appropriate for the characterisation of soft biological tissues and biomaterials in a variety of applications such as tissue engineering and disease modelling. Moreover, using data from the loading portion of the load-displacement curve and accurately identifying the initial point of contact, the nano-$\dot{\varepsilon}M$ allows the derivation of material viscoelastic properties in the absence of pre-stress.

Consequently, the estimated viscoelastic constants are representative of the mechanical behaviour of the “virgin” material and are independent of the maximum load (or displacement) chosen for the measurements, making the nano-$\dot{\varepsilon}M$ significantly advantageous over classical and widely accepted

methods based on the analysis of the unloading curve, such as the Oliver-Pharr method, or requiring a force trigger prior to starting measurements, such as CSM.

Acknowledgements

The work leading to these results has received funding from the European Union Seventh Framework Programme (FP7/2007-2013) under grant agreement 304961 (ReLiver).

Conflicts of interest

GM and AA declare no conflicts of interest. GG and NR are employees/shareholders of Optics 11.

References

Albert, C., Jameson, J., Toth, J.M., Smith, P., Harris, G., 2013. Bone properties by nanoindentation in mild and severe osteogenesis imperfecta. Clin. Biomech. (Bristol, Avon) 28, 110–6. doi:10.1016/j.clinbiomech.2012.10.003

Basu, S., Moseson, A., Barsoum, M.W., 2006. On the determination of spherical nanoindentation stress--strain curves. J. Mater. Res. 21, 2628–2637.

Bigi, A., Cojazzi, G., Panzavolta, S., Rubini, K., Roveri, N., 2001. Mechanical and thermal properties of gelatin films at different degrees of glutaraldehyde crosslinking. Biomaterials 22, 763–8.

Bouaita, N., Bull, S.J., Palacio, J.F., White, J.R., 2006. Dynamic nanoindentation of some polyolefins. Polym. Eng. Sci. 46, 1160–1172. doi:10.1002/pen.20596

Cao, Y., Yang, D., Soboyejoy, W., 2011. Nanoindentation Method for Determining the Initial Contact and Adhesion Characteristics of Soft Polydimethylsiloxane. J. Mater. Res. 20, 2004–2011. doi:10.1557/JMR.2005.0256

Chavan, D., Van De Watering, T.C., Gruca, G., Rector, J.H., Heeck, K., Slaman, M., Iannuzzi, D., 2012. Ferrule-top nanoindenter: An optomechanical fiber sensor for nanoindentation. Rev. Sci. Instrum. 83. doi:10.1063/1.4766959

Chen, Z.-W., Joli, P., Feng, Z.-Q., 2015. Anisotropic hyperelastic behavior of soft biological tissues. Comput. Methods Biomech. Biomed. Engin. 18, 1436–44. doi:10.1080/10255842.2014.915082

Chiravarambath, S., Simha, N.K., Namani, R., Lewis, J.L., 2009. Poroviscoelastic cartilage properties in the mouse from indentation. J. Biomech. Eng. 131, 011004. doi:10.1115/1.3005199

Constantinides, G., Ravi Chandran, K.S., Ulm, F.-J., Van Vliet, K.J., 2006. Grid indentation analysis of composite microstructure and mechanics: Principles and validation. Mater. Sci. Eng. A 430, 189–202. doi:10.1016/j.msea.2006.05.125

Cuy, J.L., Mann, A.B., Livi, K.J., Teaford, M.F., Weihs, T.P., 2002. Nanoindentation mapping of the mechanical properties of human molar tooth enamel. Arch. Oral Biol. 47, 281–291. doi:10.1016/S0003-9969(02)00006-7

Derby, B., Akhtar, R. (Eds.), 2015. Mechanical Properties of Aging Soft Tissues, Engineering Materials and Processes. Springer International Publishing, Cham. doi:10.1007/978-3-319-03970-1

DeWall, R.J., Bharat, S., Varghese, T., Hanson, M.E., Agni, R.M., Kliewer, M. a, 2012. Characterizing the compression-dependent viscoelastic properties of human hepatic pathologies using dynamic compression testing. Phys. Med. Biol. 57, 2273–86. doi:10.1088/0031-9155/57/8/2273

Ebenstein, D.M., Pruitt, L.A., 2004. Nanoindentation of soft hydrated materials for application to vascular tissues. J. Biomed. Mater. Res. A 69, 222–32. doi:10.1002/jbm.a.20096

Ebenstein, D.M., Pruitt, L.A., 2006. Nanoindentation of biological materials. Nano Today 1, 26–33. doi:10.1016/S1748-0132(06)70077-9

Eberhardsteiner, L., Hellmich, C., Scheiner, S., 2014. Layered water in crystal interfaces as source for bone viscoelasticity: arguments from a multiscale approach. Comput. Methods Biomech. Biomed. Engin. 17, 48–63.

Field, J.S., Swain, M.V., 1993. A simple predictive model for spherical indentation. J. Mater. Res. doi:10.1557/JMR.1993.0297

Field, J.S., Swain, M.V., 1995. Determining the mechanical properties of small volumes of material from submicrometer spherical indentations. J. Mater. Res. doi:10.1557/JMR.1995.0101

Franke, O., Göken, M., Meyers, M.A., Durst, K., Hodge, A.M., 2011. Dynamic nanoindentation of articular porcine cartilage. Mater. Sci. Eng. C 31, 789–795. doi:10.1016/j.msec.2010.12.005

Galli, M., Comley, K.S.C., Shean, T.A.V., Oyen, M.L., 2011a. Viscoelastic and poroelastic mechanical characterization of hydrated gels. J. Mater. Res. 24, 973–979. doi:10.1557/jmr.2009.0129

Galli, M., Fornasiere, E., Cugnoni, J., Oyen, M.L., 2011b. Poroviscoelastic characterization of particle-reinforced gelatin gels using indentation and homogenization. J. Mech. Behav. Biomed. Mater. 4, 610–7. doi:10.1016/j.jmbbm.2011.01.009

Gentleman, E., Swain, R.J., Evans, N.D., Boonrungsiman, S., Jell, G., Ball, M.D., Shean, T.A. V, Oyen, M.L., Porter, A., Stevens, M.M., 2009. Comparative materials differences revealed in engineered bone as a function of cell-specific differentiation. Nat. Mater. 8, 763–70. doi:10.1038/nmat2505

Gray, D.S., Tien, J., Chen, C.S., 2003. Repositioning of cells by mechanotaxis on surfaces with micropatterned Young's modulus. J. Biomed. Mater. Res. A 66, 605–14. doi:10.1002/jbm.a.10585

Haghshenas, M., Klassen, R.J., 2013. Assessment of the depth dependence of the indentation stress during constant strain rate nanoindentation of 70/30 brass. Mater. Sci. Eng. A 572, 91–97. doi:10.1016/j.msea.2013.02.009

Hayes, S.A., Goruppa, A.A., Jones, F.R., 2011. Dynamic nanoindentation as a tool for the examination of polymeric materials. J. Mater. Res. 19, 3298–3306. doi:10.1557/JMR.2004.0437

Herbert, E.G., Pharr, G.M., Oliver, W.C., Lucas, B.N., Hay, J.L., 2001. On the measurement of stress-strain curves by spherical indentation. Thin Solid Films 398-399, 331–335. doi:10.1016/S0040-6090(01)01439-0

Hollister, S.J., Jeong, C.G., Schwiedrzik, J.J., Mitsak, A.G., Kang, H., Migneco, F., 2011. Nonlinear Elastic Scaffold Design, Modeling and Fabrication for Soft Tissue Engineering, in: Advances on Modeling in Tissue Engineering. Springer, pp. 35–53.

Hu, Y., Zhao, X., Vlassak, J.J., Suo, Z., 2010. Using indentation to characterize the poroelasticity of gels. Appl. Phys. Lett. 96, 121904. doi:10.1063/1.3370354

Kalyanam, S., Yapp, R.D., Insana, M.F., 2009. Poro-viscoelastic behavior of gelatin hydrogels under compression-implications for bioelasticity imaging. J. Biomech. Eng. 131, 081005. doi:10.1115/1.3127250

Karimzadeh, A., Ayatollahi, M.R., 2014. Mechanical properties of biomaterials determined by nano-indentation and nano-scratch tests, in: Nanomechanical Analysis of High Performance Materials. Springer, pp. 189–207.

Kaufman, J.D., Klapperich, C.M., 2009. Surface detection errors cause overestimation of the modulus in nanoindentation on soft materials. J. Mech. Behav. Biomed. Mater. 2, 312–317. doi:10.1016/j.jmbbm.2008.08.004

Kaufman, J.D., Miller, G.J., Morgan, E.F., Klapperich, C.M., 2008. Time-dependent mechanical characterization of poly(2-hydroxyethyl methacrylate) hydrogels using nanoindentation and unconfined compression. J. Mater. Res. 23, 1472–1481. doi:10.1557/JMR.2008.0185

Khanafer, K., Duprey, A., Schlicht, M., Berguer, R., 2009. Effects of strain rate, mixing ratio, and stress-strain definition on the mechanical behavior of the polydimethylsiloxane (PDMS) material as related to its biological applications. Biomed. Microdevices 11, 503–508. doi:10.1007/s10544-008-9256-6

Kwon, J., Subhash, G., 2010. Compressive strain rate sensitivity of ballistic gelatin. J. Biomech. 43, 420–5. doi:10.1016/j.jbiomech.2009.10.008

Li, X., Bhushan, B., 2002. A review of nanoindentation continuous stiffness measurement technique and its applications. Mater. Charact. 48, 11–36. doi:10.1016/S1044-5803(02)00192-4

Lin, I.-K., Ou, K.-S.S., Liao, Y.-M., Liu, Y., Chen, K.-S.-S., Zhang, X., 2009. Viscoelastic Characterization and Modeling of Polymer Transducers for Biological Applications. J. Microelectromechanical Syst. 18, 1087–1099. doi:10.1109/JMEMS.2009.2029166

Lin, Y.-Y., Hu, B.-W., 2006. Load relaxation of a flat rigid circular indenter on a gel half space. J. Non. Cryst. Solids 352, 4034–4040. doi:10.1016/j.jnoncrysol.2006.07.007

Lucas, B.N., Oliver, W.C., Pharr, G.M., Loubet, J.-L., 2011. Time Dependent Deformation During Indentation Testing. MRS Proc. 436, 233. doi:10.1557/PROC-436-233

Lyyra, T., Jurvelin, J., Pitkänen, P., Väätäinen, U., Kiviranta, I., 1995. Indentation instrument for the measurement of cartilage stiffness under arthroscopic control. Med. Eng. Phys. 17, 395–9.

Maier, V., Durst, K., Mueller, J., Backes, B., Höppel, H.W., Göken, M., 2011. Nanoindentation strain-rate jump tests for determining the local strain-rate sensitivity in nanocrystalline Ni and ultrafine-grained Al. J. Mater. Res. 26, 1421–1430. doi:10.1557/jmr.2011.156

Mak, A.F., Lai, W.M., Mow, V.C., 1987. Biphasic indentation of articular cartilage--I. Theoretical analysis. J. Biomech. 20, 703–14.

Mann, A.B., Pethica, J.B., 1996. Nanoindentation Studies in a Liquid Environment †. Langmuir 12, 4583–4586. doi:10.1021/la950901z

Martucci, J.F., Ruseckaite, R.A., Vázquez, A., 2006. Creep of glutaraldehyde-crosslinked gelatin films. Mater. Sci. Eng. A 435-436, 681–686. doi:10.1016/j.msea.2006.07.097

Mattei, G., Ferretti, C., Tirella, A., Ahluwalia, A., Mattioli-Belmonte, M., 2015. Decoupling the role of stiffness from other hydroxyapatite signalling cues in periosteal derived stem cell differentiation. Sci. Rep. 5, 10778. doi:10.1038/srep10778

Mattei, G., Tirella, A., Gallone, G., Ahluwalia, A., 2014. Viscoelastic characterisation of pig liver in unconfined compression. J. Biomech. 47, 2641–6. doi:10.1016/j.jbiomech.2014.05.017

Olesiak, S.E., Sponheimer, M., Eberle, J.J., Oyen, M.L., Ferguson, V.L., 2010. Nanomechanical properties of modern and fossil bone. Palaeogeogr. Palaeoclimatol. Palaeoecol. 289, 25–32. doi:10.1016/j.palaeo.2010.02.006

Oliver, W.C., Pharr, G.M., 1992. An improved technique for determining hardness and elastic modulus using load and displacement sensing indentation experiments. J. Mater. Res. doi:10.1557/JMR.1992.1564

Oliver, W.C., Pharr, G.M., 2004. Measurement of hardness and elastic modulus by instrumented indentation: Advances in understanding and refinements to methodology. J. Mater. Res. 19, 3–20. doi:10.1557/jmr.2004.19.1.3

Oyen, M.L., 2013. Nanoindentation of biological and biomimetic materials. Exp. Tech. 37, 73–87. doi:10.1111/j.1747-1567.2011.00716.x

Oyen, M.L., Cook, R.F., 2003. Load–displacement behavior during sharp indentation of viscous–elastic–plastic materials. J. Mater. Res. doi:10.1557/JMR.2003.0020

Oyen, M.L., Cook, R.F., 2009. A practical guide for analysis of nanoindentation data. J. Mech. Behav. Biomed. Mater. 2, 396–407. doi:10.1016/j.jmbbm.2008.10.002

Pathak, S., Kalidindi, S.R., Klemenz, C., Orlovskaya, N., 2008a. Analyzing indentation stress-strain response of LaGaO3 single crystals using spherical indenters. J. Eur. Ceram. Soc. 28, 2213–2220. doi:10.1016/j.jeurceramsoc.2008.02.009

Pathak, S., Kalidindi, S.R., Moser, B., Klemenz, C., Orlovskaya, N., 2008b. Analyzing indentation behavior of LaGaO3 single crystals using sharp indenters. J. Eur. Ceram. Soc. 28, 2039–2047. doi:10.1016/j.jeurceramsoc.2008.02.010

Radmacher, M., Fritz, M., Hansma, P.K., 1995. Imaging soft samples with the atomic force microscope: gelatin in water and propanol. Biophys. J. 69, 264–70. doi:10.1016/S0006-3495(95)79897-6

Raghunathan, S., Evans, D., Sparks, J.L., 2010. Poroviscoelastic modeling of liver biomechanical response in unconfined compression. Ann. Biomed. Eng. 38, 1789–800. doi:10.1007/s10439-010-9957-x

Rettler, E., Hoeppener, S., Sigusch, B.W., Schubert, U.S., 2013. Mapping the mechanical properties of biomaterials on different length scales: depth-sensing indentation and AFM based nanoindentation. J. Mater. Chem. B 1, 2789. doi:10.1039/c3tb20120a

Sasaki, S., 2004. Stress relaxation of deformed gel in a good solvent. J. Chem. Phys. 120, 5789–94. doi:10.1063/1.1649933

Scheiner, S., Hellmich, C., 2009. Continuum Microviscoelasticity Model for Aging Basic Creep of Early-Age Concrete. J. Eng. Mech. 135, 307–323. doi:10.1061/(ASCE)0733-9399(2009)135:4(307)

Shen, L., Cheong, W.C.D., Foo, Y.L., Chen, Z., 2012. Nanoindentation creep of tin and aluminium: A comparative study between constant load and constant strain rate methods. Mater. Sci. Eng. A 532, 505–510. doi:10.1016/j.msea.2011.11.016

Simha, N.K., Jin, H., Hall, M.L., Chiravarambath, S., Lewis, J.L., 2007. Effect of indenter size on elastic modulus of cartilage measured by indentation. J. Biomech. Eng. 129, 767–75. doi:10.1115/1.2768110

Sneddon, I.N., 1965. The relaxation between load and penetration in the axisymmetric Boussinesq problem for a punch of arbitrary profile. Int. J. Eng. Sci. 3, 47–57.

Tabor, D., 1951. The hardness of metals. Clarendon Press, Oxford.

Tirella, A., Mattei, G., Ahluwalia, A., 2014. Strain rate viscoelastic analysis of soft and highly hydrated biomaterials. J. Biomed. Mater. Res. A 102, 3352–60. doi:10.1002/jbm.a.34914